Sensor and Simulation Notes

Note 480

November 10, 2003

JOLT: A Highly Directive, Very Intensive, Impulse-Like Radiator

Carl E. Baum, William L. Baker, William D. Prather, William A. Walton III,
Ronald Hackett, Jane M. Lehr[1], Jeffrey W. Burger, Robert J. Torres, James O'Loughlin
Harald A. Dogliani[2], J. Scott Tyo[3], and Jon S.H.Schoenberg[4], Gerry J. Rohwein[5]
Air Force Research Laboratory, Directed Energy Directorate, Kirtland AFB, NM 87117

D. V. Giri
Pro-Tech, 11-C Orchard Court, Alamo, CA 94507-1541

Ian D. Smith, R. Altes, G. Harris, James Fockler,[6] and David F. Morton
Titan Pulse Sciences, Inc., 2700 Merced Street, San Leandro, CA 94577

Donald McLemore, Kelvin S. H. Lee, Terry Smith, and Howard LaValley
ITT Industries, AES Division, 5901 Indian School NE, Albuquerque, NM 87110

Michael D. Abdalla and Michael C. Skipper
ASR Corporation, 7817 Bursera NW, Albuquerque, NM 87120

Fred Gruner[7] and Brett Cockreham[8]
Kinetech, Albuquerque, NM

and

Everett G. Farr
Farr Research, Inc., 614 Paseo Del Mar NE, Albuquerque, NM 87123

---

1. Presently at Sandia National Laboratories, Albuquerque, NM.
2. Presently at Los Alamos National Laboratories, Los Alamos, NM.
3. Presently at University of New Mexico, Albuquerque, NM.
4. Presently at National Security Agency, Washington, DC.
5. Consultant, Albuquerque, NM
6. Deceased.
7. Presently at Titan / PSI, San Leandro, CA.
8. Presently with Solid Design, Inc., Albuquerque, NM.

This work was sponsored in part by the Air Force Office of Scientific Research, and in part by the Air Force Research Laboratory, Directed Energy Directorate.

Abstract

Ultra-wideband (UWB) systems that radiate very high-level transient waveforms and exhibit operating bandwidths of over two decades are now in demand for a number of applications. Such systems are known to radiate impulse-like waveforms with risetimes around 100 picoseconds (ps) and peak electric field values of 10s of kV/m. Such waveforms, if properly radiated, will exhibit an operating spectrum of over two decades, making them ideal for applications such as concealed object detection, countermine, transient radar, and communications.

In this note, we describe a large, high voltage transient system built at the Air Force Research Laboratory, Kirtland AFB, NM, during 1997-1999. The pulsed power system centers around a very compact resonant transformer capable of generating over 1 MV at a pulse repetition frequency (PRF) of 600 Hz. This is switched via an integrated transfer capacitor and an oil peaking switch onto an 85-W Half-IRA (Impulse Radiating Antenna). This unique system will deliver a far radiated field with a full-width half maximum (FWHM) on the order of 100 ps, and a field-range product ($r\ E_{far}$) of ~ 5.3 MV, exceeding all previously reported results by a factor of several.

Contents

1. Introduction

Many high-power transient sources (100's of kV in amplitude, 50-200 ps risetimes) that employ oil or gas spark-gap switches are designed and fabricated with coaxial or single-ended output geometry [1]. In addition, solid-state transient sources [2-4] are also commercially available with typically 50 Ω coaxial cable output. A full reflector type of an impulse radiating antenna (IRA) [5-8], shown schematically in figure 1 requires a differential TEM feed to avoid common mode currents on the feed plates, which adversely impact the radiated pulse fidelity. One can get around this problem, by using a balun that converts a single-ended source into a differential feed required by a full reflector [9]. Another option with single-ended sources is to use the half IRA (HIRA) [10-13]. The 3.66m (or 12 feet diameter) prototype IRA [5, 6] happens to be the first reflector IRA that was ever built and it had incorporated a differential feed by the use of a center-tapped pulse transformer in its source design. Some examples of full IRAs that are presently being used are summarized in Table 1.

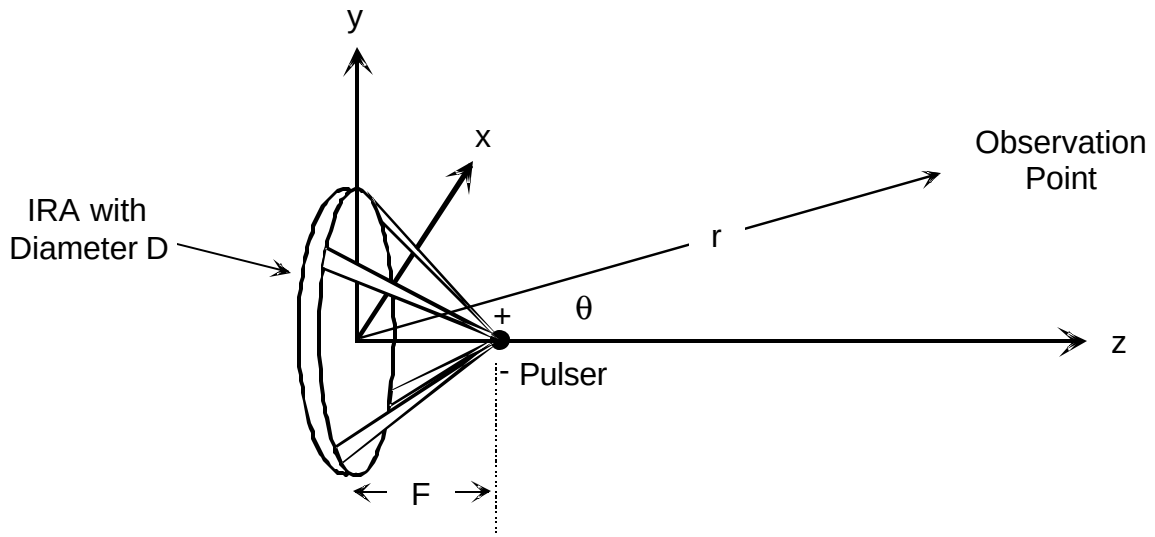

Figure 1. Line schematic of a reflector type of an Impulse Radiating Antenna (IRA)

It is observed from Table 1 that the band ratio (the ratio of high to low frequencies between which the radiated spectrum is fairly flat) is > 10 which makes all of these hyperband [14] radiating systems.

TABLE 1. Examples of Impulse Radiating Antennas

#	Name	Pulser	Antenna	Near field	Far field	r E_{far}	r E_{far}/ V_o	Band Ratio br
1	Prototype IRA AFRL, KAFB, NM USA	± 60 kV 100ps/20ns 200 HZ burst	3.66m dia (F/D)=0.33	23 kV/m at r = 2m	4.2 kV/m at r = 304m	1280 kV	10.67	100
2	Upgraded prototype IRA AFRL, KAFB, NM USA	± ~ 75 kV 85 ps/ 20 ns ~ 400 HZ	1.83 m dia (F/D)=0.33	41.6 kV/m at r = 16.6m	27.6 kV/m at r = 25 m	690 kV	5 to 6 (est.)	50
3	Swiss IRA NEMP Laboratory Spiez, Switzerland	2.8 kV 100 ps / 4 ns 800 Hz	1.8 m dia (F/D)=0.28	1.4 kV/m at r = 5m	220 V/m at r = 41 m	10 kV	4	50
4	TNO IRA The Hague Netherlands	9 kV 100 ps / 4 ns 800 Hz	0.9 m dia (F/D)=0.37	7 kV/m at r = 1m	3.4 kV/m at r = 10m	34 kV	3	25
5	Univ. of Magdeburg Magdeburg, Germany	9 kV 100 ps / 4 ns 800 Hz	0.9 m dia (F/D)=0.37	7 KV/m at r =1m	3.4 kV/m at r = 10m	34 kV	3 (est.)	25

Hyperband systems exemplified in Table 1 that radiate very high-level transient waveforms and exhibit operating bandwidths of 1 to 2 decades are now in demand for a number of applications. Such systems are known to radiate impulse-like waveforms with risetimes around 100 picoseconds (ps) and peak electric field values of 10s of kV/m. Such waveforms, if properly radiated, will exhibit an operating spectrum of over two decades, making them ideal for applications such as concealed object detection, countermine, transient radar, and communications.

In this note, we describe a large, high voltage transient system built at the Air Force Research Laboratory, Kirtland AFB, NM, during 1997-1999. The pulsed power system centers around a very compact resonant transformer capable of generating over 1 MV at a pulse repetition rate PRF of 600 Hz. This is switched, via an integrated transfer capacitor and an oil peaking switch onto an 85-W Half-IRA (Impulse Radiating Antenna). This unique system will deliver a far radiated field with FWHM on the order of 100 ps, and a field-range product (r E_{far}) of ~ 5.3 MV, exceeding all previously reported results by a factor of several.

2. Components of the Overall System

The JOLT half-IRA is exactly half of a paraboloidal reflector antenna which is fed by a pair of conical transmission lines. In other words, it is the top half of the antenna shown in figure 1, as shown conceptually in figure 2. Each TEM feed line has a characteristic impedance of 170 Ω (in oil) against the image plane, resulting in a net antenna impedance of 85 Ω for all frequencies, as long as TEM launch condition is maintained. It is then possible to think of the antenna system as a "85 Ω load" energized by the pulser. Typically the energy is stored in a capacitor and switched out to the antenna which is seen as load by the pulser, as indicated in figure 3.

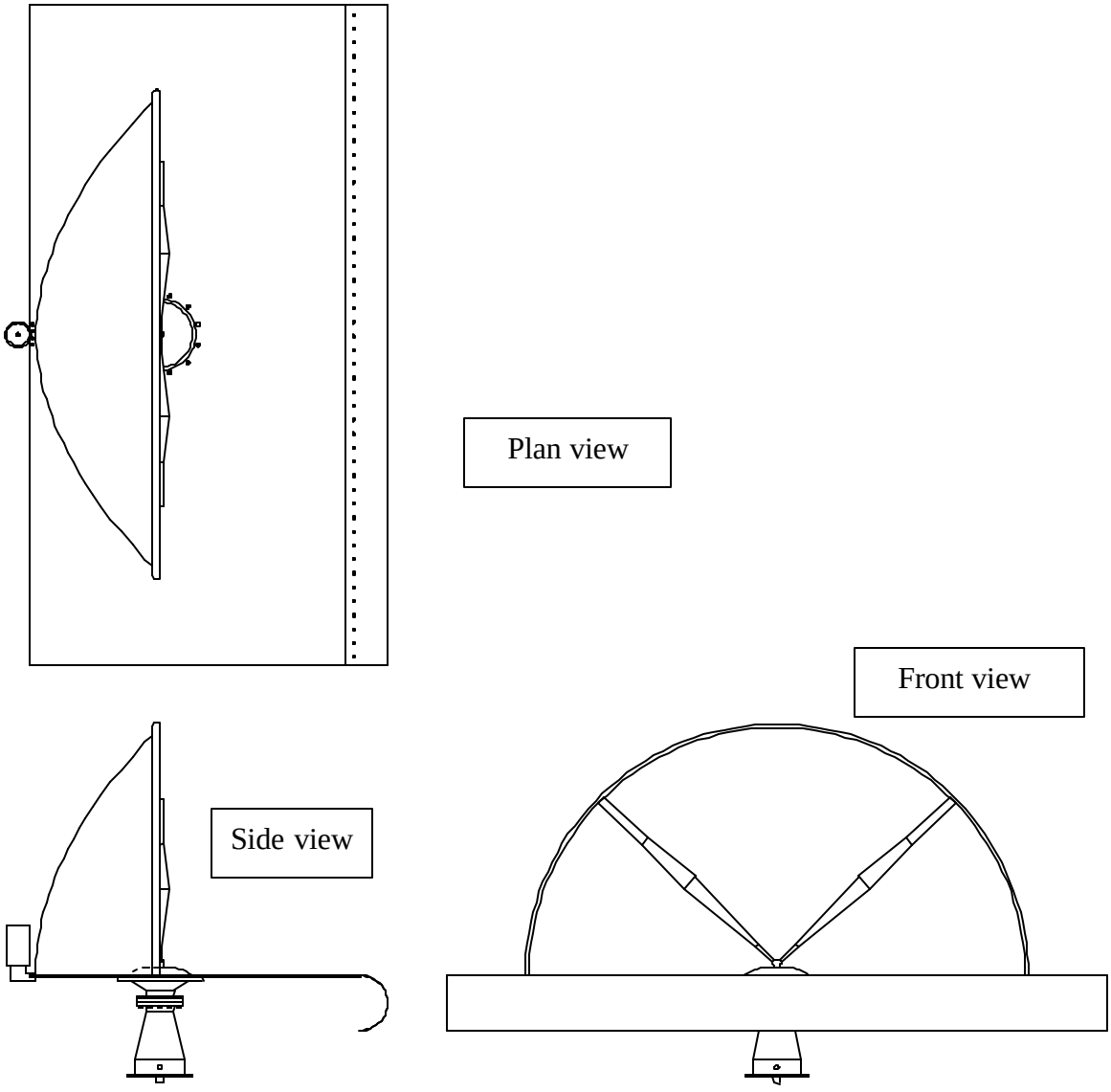

Figure 2. Line Schematic diagram of the HIRA, showing all three views

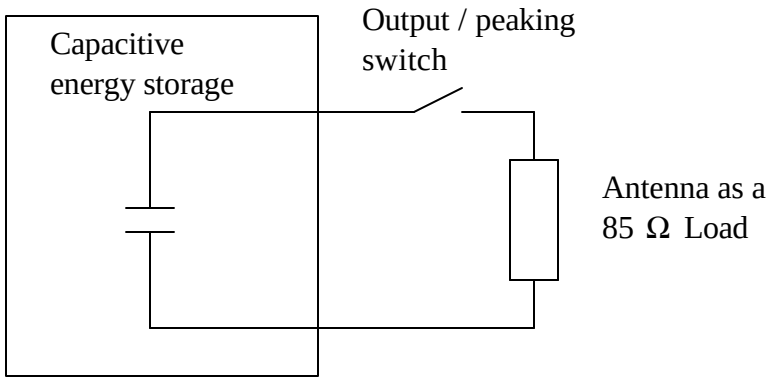

Figure 3. Capacitively stored transient energy switched-out to the antenna

The hyperband HIRA that will be described in the following sections has been called the JOLT and its pulser has many stages starting from the prime-power to the final peaking switch that switches out the transient energy to the antenna. Introducing these stages of the pulser, figure 3 is redrawn as a block–schematic diagram in figure 4.

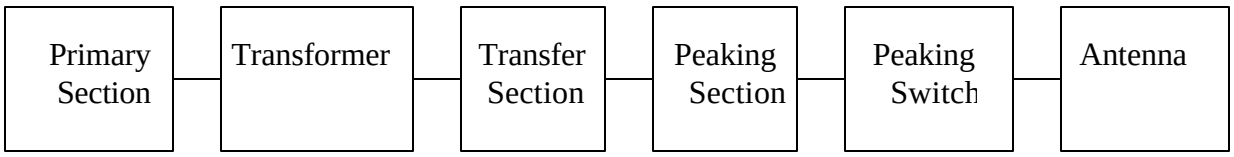

Figure 4. Block-schematic diagram of JOLT system

The overall equivalent circuit of the system can be seen in Figure 5. The first four blocks in figure 4 extending from the primary section to the peaking section are regarded as pulser components, while the peaking switch located at or near the focal point of the reflector antenna is what interfaces the pulser to the antenna. In this sense, the peaking switch can be regarded as the "source of transient energy", because the instant the peaking switch closes, one can say the fast and intensive pulse is launched on to the conical transmission lines that guide a spherical TEM wave to illuminate the paraboloidal reflector. It is also observed from figure 5 that the equivalent circuit for the various stages of the pulser consists primarily of lumped elements (diodes, resistors, inductors, and capacitors), pulse transformers and switches. Transmission lines either two-wire or coaxial are also part of pulser equivalent circuit and such lines are also simulated by cascaded L-C sections as seen in figure 5.

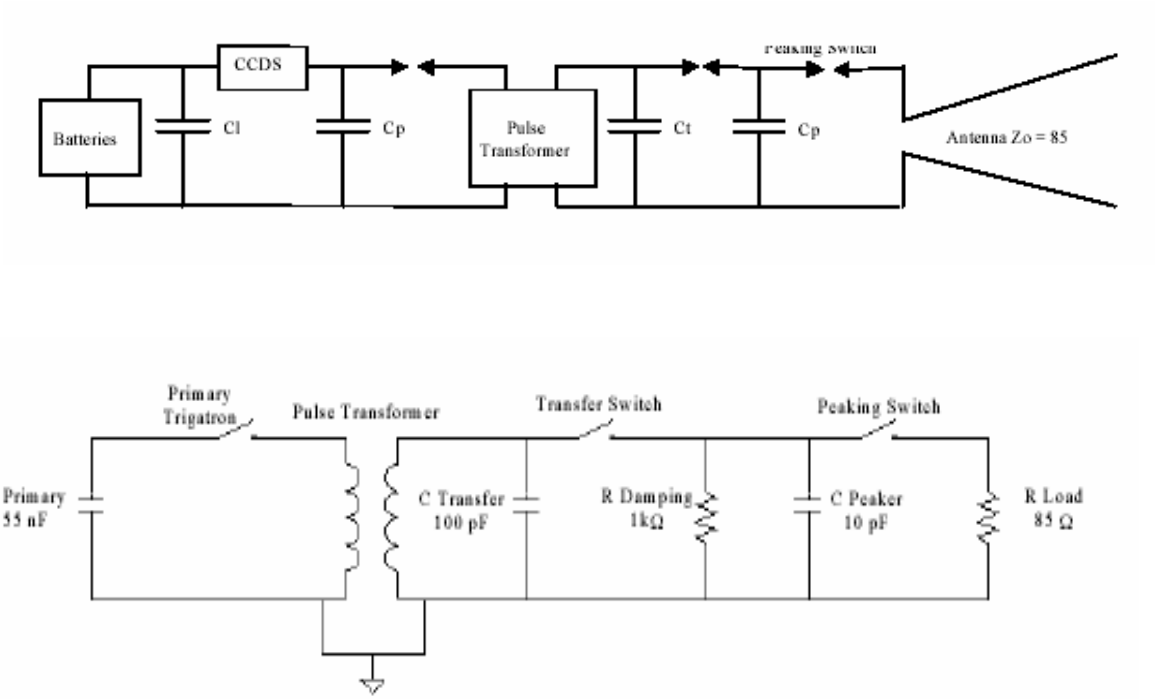

Figure 5. Different forms of the equivalent circuit for the JOLT hyperband system

On the other hand, the antenna is an electromagnetically complex system to analyze. The antenna is symbolically represented by its frequency independent input impedance (85 Ω load) as shown in figure 5. One can reach an inescapable conclusion that:

- High-voltage transient pulsers generating 100's of kV in ~ 100 ps with (dV/dt) of $\geq 10^{15}$ V/s are hard to design and fabricate, but relatively easy to analyze via electrical circuits with lumped and distributed components,
- in contra distinction, the antennas driven by such pulsers are passive and easy to fabricate since they tend to be a collection of simple conductors, resistors and dielectrics, but can be very complex to analyze via the solution of Maxwell's equations under appropriate boundary conditions.

In section 3, we will describe the various pulser components, followed by a description of the radiator in Section 4.

3. Various Pulser Components

The various stages of the pulser as a whole were identified in figure 4 and are individually described in what follows.

3.1 Primary Section

The primary energy storage is a 55 nF, rectangular co-axial capacitor bank as shown in figure 6. A co-axial geometry was chosen for minimum inductance. Ring-down measurements into a short-circuit indicate that the entire energy storage assembly has an inductance of approximately 100 nH. The bank is formed with TDK ceramic capacitors mounted between inner and outer aluminum conductors. The outer conductor is fabricated from 0.060" thick aluminum and the inner conductor is fabricated from 0.5" thick aluminum. There are 32 TDK model UHV-12A capacitors in the assembly. Each capacitor is rated at 1.72 nF and 50 kV hold-off in air. The aluminum rectangular co-axial structure is contained within a dielectric box made of 0.5" thick acrylic. The entire assembly is filled with Dow Corning Sylgard 184 silicone elastomer for dielectric protection. The outer dimensions of the acrylic box are 16" x 11.5" x 6" and the entire assembly weighs approximately 75 pounds.

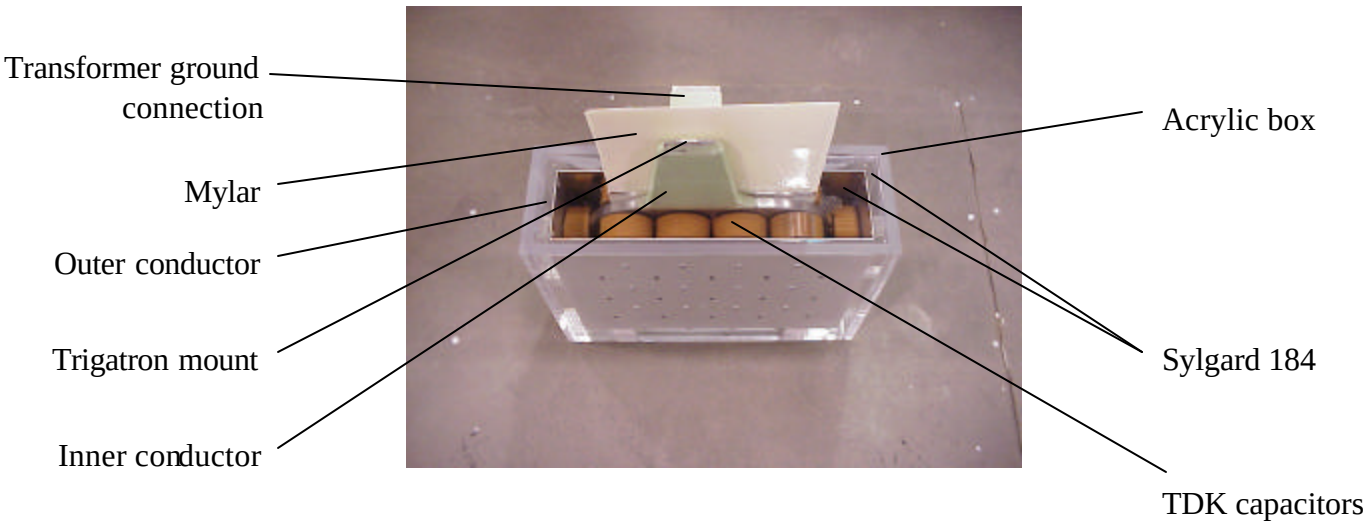

Figure 6. Primary power stored in a rectangular coaxial bank of capacitors

The capacitor bank center conductor narrows to a mounting flange that attaches to the un-triggered side of the trigatron. The capacitor bank outer conductor has a strap that connects to the ground side of the dual resonant transformer input. Each of these electrical connections is coated with Sylastic Type J two-part elastomer to suppress corona. In addition, multiple sheets of Mylar are installed to prevent surface flashover along the Sylgard 184 between the connections. The 8 CCDS power supplies charge the capacitor bank to 50 kV in approximately 900 μs. The trigaton is triggered approximately 400 μs later which discharges the capacitor bank into the primary of the dual resonant transformer.

The trigatron, shown in figure 7 is a triggered hydrogen switch designed for high repetition rate operation at up to 50 kV charge voltage in air. The switch electrodes are designed as a Rogowski profile for uniform field distribution and are fabricated of copper-tungsten for maximum lifetime. The main gap spacing is 0.17" and the trigger pin is spaced 0.085" from the ground electrode. Each electrode is supported by end plates that are fabricated from 7075 "aircraft" aluminum. The trigger pin is also fabricated from copper-tungsten and is threaded to the tip of a modified automotive spark plug. The spark plug is threaded into the ground-side end plate and the standard spark plug copper gasket serves as the pressure seal. The spark plug serves to electrically isolate the trigger from the end plate. A two-piece outer shell is made of G-10 and screws together to clamp the end plates against a KEL-F insert. The end plates seal to the KEL-F insert using two polysulfide O-rings. The KEL-F insert was chosen because of its low permeability for hydrogen and its resistance to damage by UV radiation from the arc.

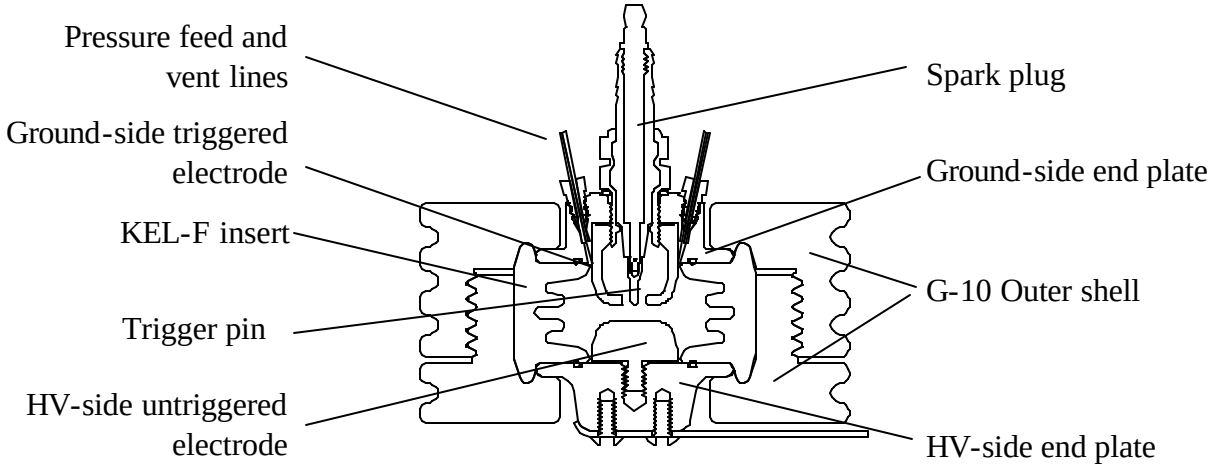

(a) Line schematic

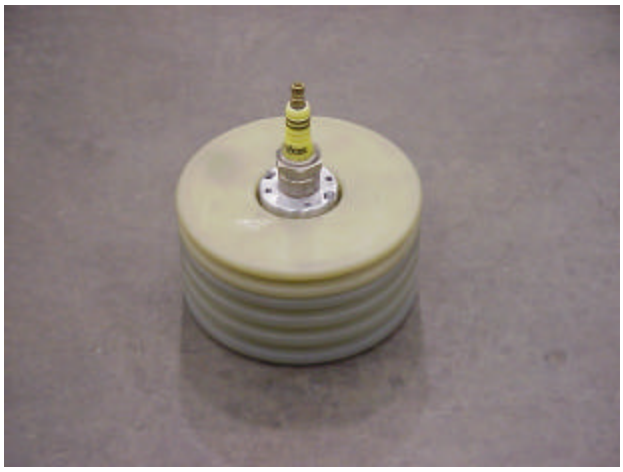

(b) Photograph

Figure 7. Schematic diagram and photograph of the triggered hydrogen switch designed for high repetition rate

In the JOLT system, the trigatron is operated at approximately 300 psig and is designed to have a 4:1 safety factor at 1,000 psig. Additional details and the development of the trigatron switch for high repetition rate operation may be found in [15].

3.2 Transformer Section

The pulse transformer shown is a dual-resonant, flat wound design and provides a 22:1 voltage ring-up ratio from the energy storage capacitor bank to the transfer capacitor. The turns ratio of 22:1 steps up the 50 kV to a maximum of 1.1 MV. The transformer output waveform is shown in figure 8 and the transformer itself can be seen in figure 9. The transformer is designed

as an autotransformer with the outermost winding being the primary and the center section being charged to high voltage. The windings are electrically insulated with a combination of sheet Mylar, Kraft paper and dielectric oil. The outer case is made of acrylic and the top and bottom plates are made of acrylic and aluminum respectively. The center tube section serves as a routing path for the high-pressure hydrogen lines that supply the transfer switch.

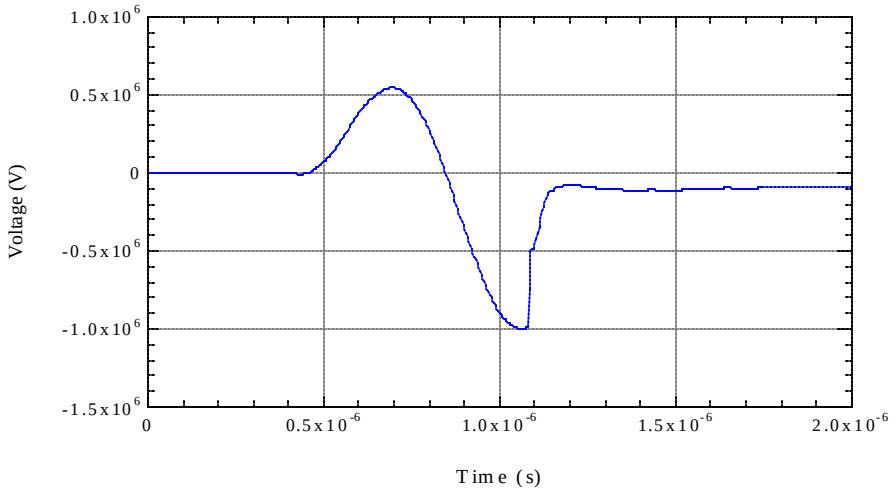

Figure 8. A representative output voltage waveform from the pulse transformer

It is noted that this particular waveform of figure 8 does not integrate back to 0 (derived from a measurement of (dV/dt) because we lost some data points at the very fast transient where the transfer switch closed. We did verify that when these data points are taken into account, the waveform does integrate to 0. In the above figure, the switch closure occurs at ~ 1.1 μs and normal switch closure voltages are between 1.0 and 1.1 MV.

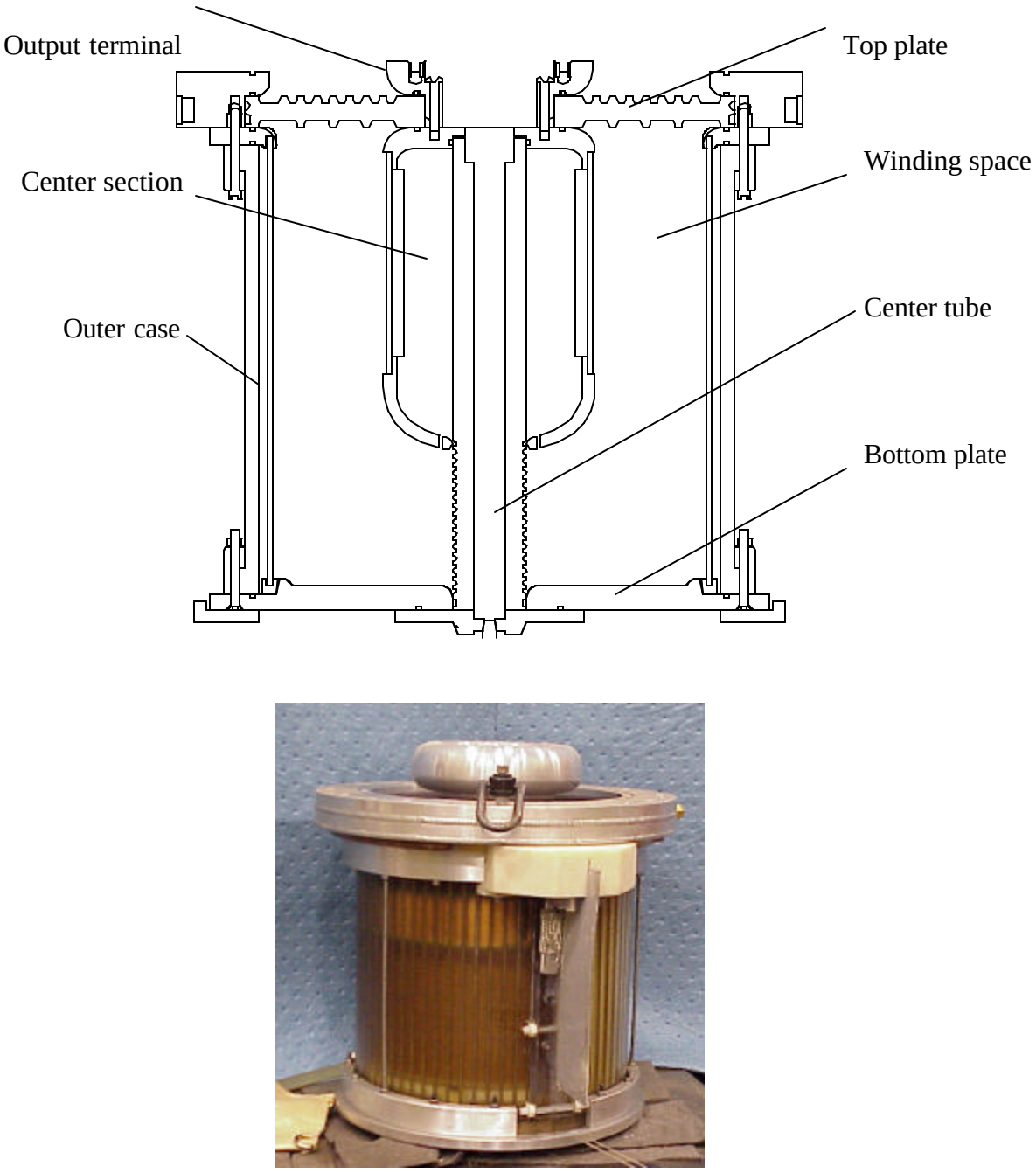

Figure 9. Line schematic and a photograph of the pulse transformer to step up the voltage from 50 kV to over 1 MV

This transformer is one of the key components of JOLT and the general design features of this pulse transformer were: (a) Compact cylindrical configuration, 0.368m inner diameter, 0.432m long, (b) vertical flange mount in the JOLT system, (c) side feeds connect to capacitor bank and switch, (d) spiral strip air core windings, (e) oil impregnated polypropylene film insulation, (f)

longitudinal coaxial electric field shapers improve system efficiency, (g) dual resonance charge transfer cycle 1.2 MV, 200 Hz operation. The electrical parameters of the transformer are summarized in Table 2.

TABLE 2. Electrical parameters of the JOLT transformer

Quantity	Measured	Calculated
Primary Inductance, μH	0.402	0.457
Secondary inductance, μH	242	286
Coupling coefficient	0.65	0.66
Winding capacitance, pF	55	--

The lifetime of early transformers was limited to approximately 1000 shots by internal breakdowns. Initial modifications to transformer design did not improve shot life. A detailed failure analysis revealed that high frequency effects in combination with high pulse repetition rates produced internal partial discharges and gas generation which led to insulator breakdowns. In a revised design, the partial discharges were suppressed with improved voltage grading and gas isolation techniques. These modifications have met the electrical requirements and resulted in greatly improved reliability and operating life.

3.3 Transfer Switch

The design of compact, high voltage switches is generally plagued by the tradeoff between reduced size and the probabilities of bulk and surface breakdown. Moreover, typical breakdown field values for wide classes of materials with desirable electrical and mechanical properties are unavailable. In the development of a compact gas switch, capable of holding off voltages of up to 1 MV at repetition rates of 100's of Hz, a criterion to insure the inhibition of surface flashover in a high pressure atmosphere has been developed. The switch is composed of copper tungsten electrodes with a coaxial Torlon pressure containment housing of length 12.7 cm and a diameter of 15.3 cm. Pulse repetition rates in the 100's of Hz are achieved by using moderately hydrogen pressures as the insulating medium. The electrodes are shaped to produce a uniform field distribution in the gap with an adjustable spacing of 0.5, 0.75 and 1.0 cm. Additional stress is put on the switch by charging with a dual-resonant pulse transformer. The final switch design took three iterations, all of which were instructive. The evolution of the switch design has been described in [16].

The transfer switch shown in figure 10 is a self-break hydrogen switch designed for high repetition rate operation at up to 1.1 MV while insulated in flowing oil. The switch electrodes are designed with a Rogowski profile for uniform field distribution and are adjusted to a 0.75 cm gap. The electrodes are fabricated from copper-tungsten. The lower electrode is electrically connected to the output terminal of the dual resonant transformer. The upper electrode is electrically connected to the peaking capacitor output section. The upper electrode support is fabricated from 7075 aluminum and is specifically shaped to move the electric field stresses into the surrounding oil dielectric. The main pressure vessel is constructed of Torlon and is threaded into the center conductor of the coaxial transfer capacitor. The inner profile of the pressure vessel is specifically contoured to maintain tangential electric field stresses at or below 135 kV/cm. The pressure vessel is designed to have a 4:1 safety factor at 2,000 psig. The switch is normally operated at 1,650 psig for closure at 1.0 MV. The equipotential plots for the final version of the transfer switch are shown in figure 11 and the critical electric fields are shown in figure 12. One can also see the transfer switch layout in these figures. The main housing is made of Torlon [9], a high performance, molding polymer known for its strength. In addition to its outstanding mechanical strength, Torlon is easy to fabricate and has excellent creep resistance and thermal stability. Electrically, the relative dielectric constant is approximately 4 and it is known to be dispersive. The dielectric strength is listed in its data sheet as 225 kV/cm or 22.5 MV/m. Torlon is commercially available only in certain diameters, so to meet a factor of safety of four for manned operation, the Torlon housing was reinforced with a band of G-10 to hold the required pressure of 1600 psi. The air gap between the Torlon and the G10 is filled with Sylgard 527.

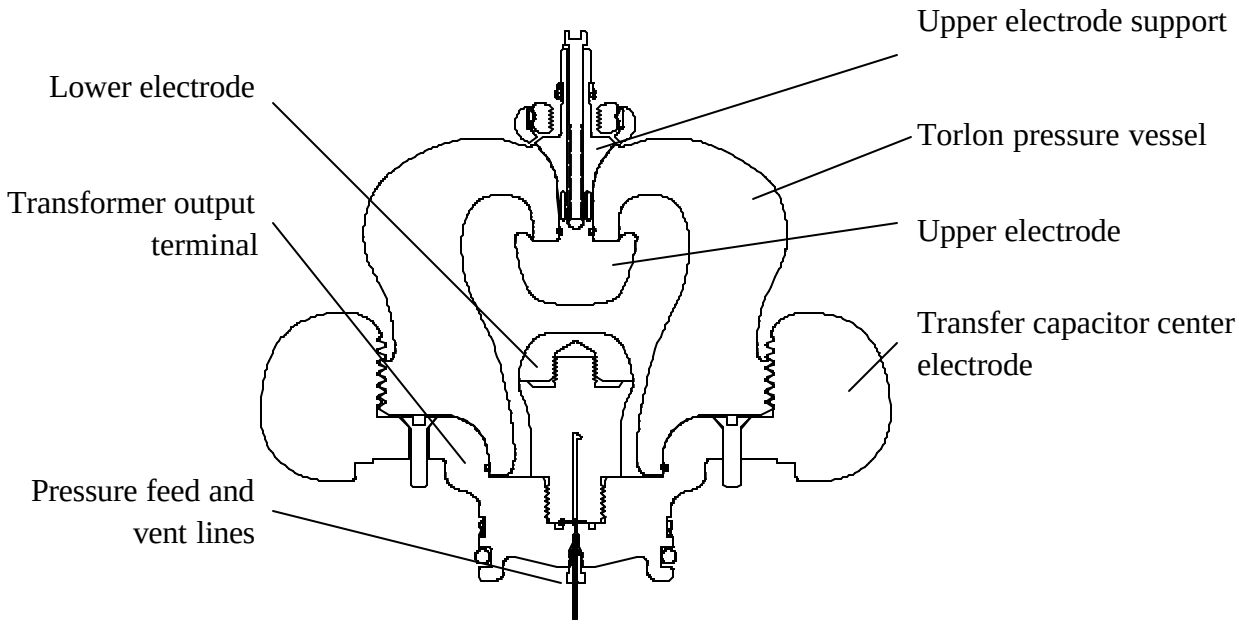

(a) Line schematic of the JOLT transfer switch

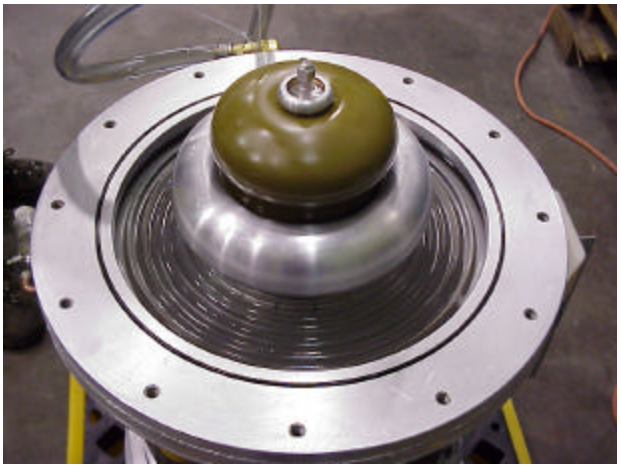

(b) Photograph of the JOLT transfer switch

Figure 10. Line schematic and photograph of the high-pressure self-breaking hydrogen transfer switch

Transfer Switch Layout

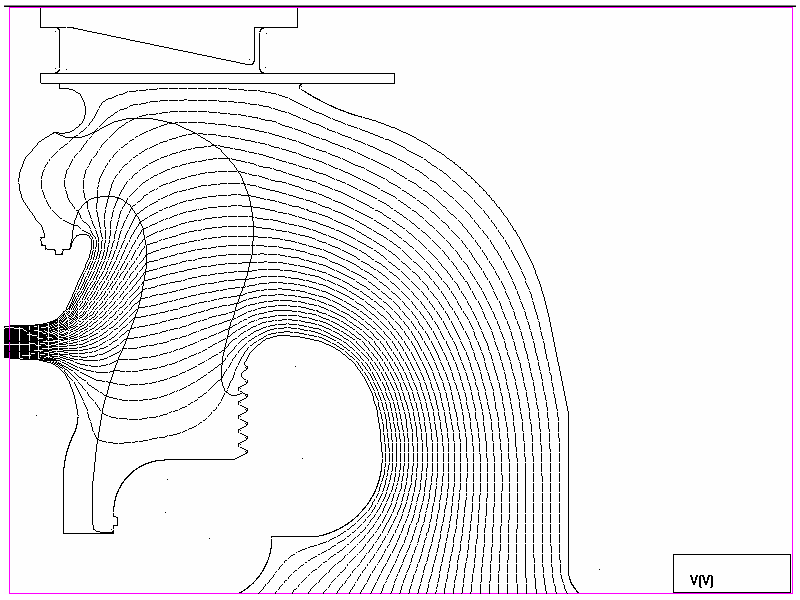

(a) JOLT transfer switch design in open mode

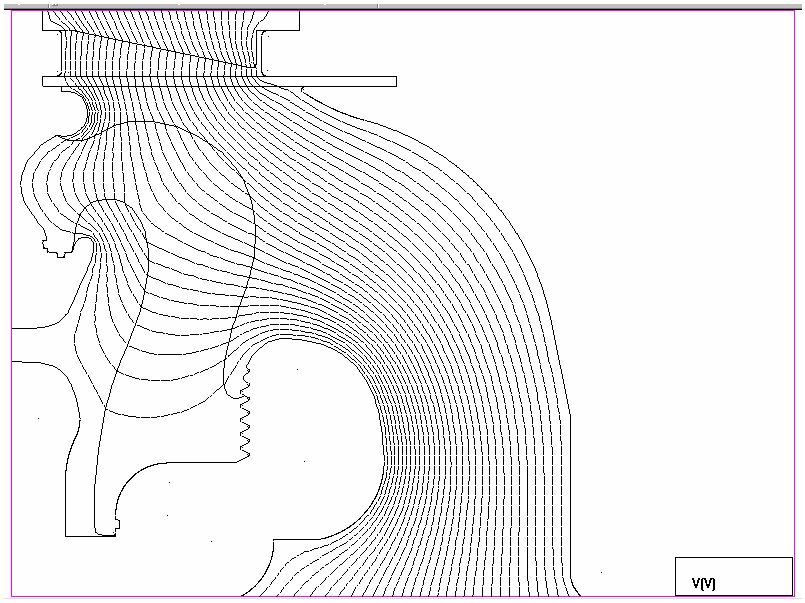

(b) JOLT transfer switch design in closed mode.

Figure 11. Equipotential plots of the JOLT transfer switch (right of the transfer switch seen in figure 10 a)

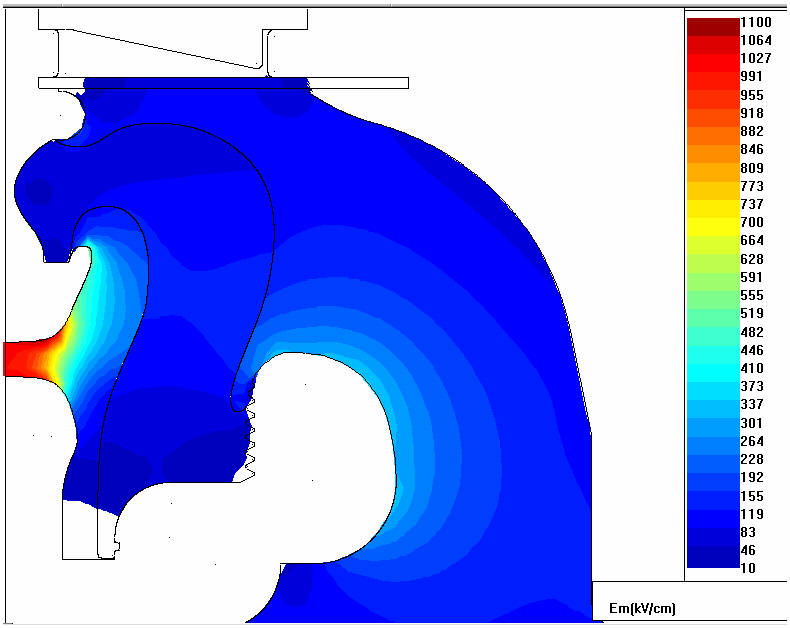

(a) Electric field distribution in JOLT transfer switch design in open mode
Note that the color graphs of (a) and (b) are different.

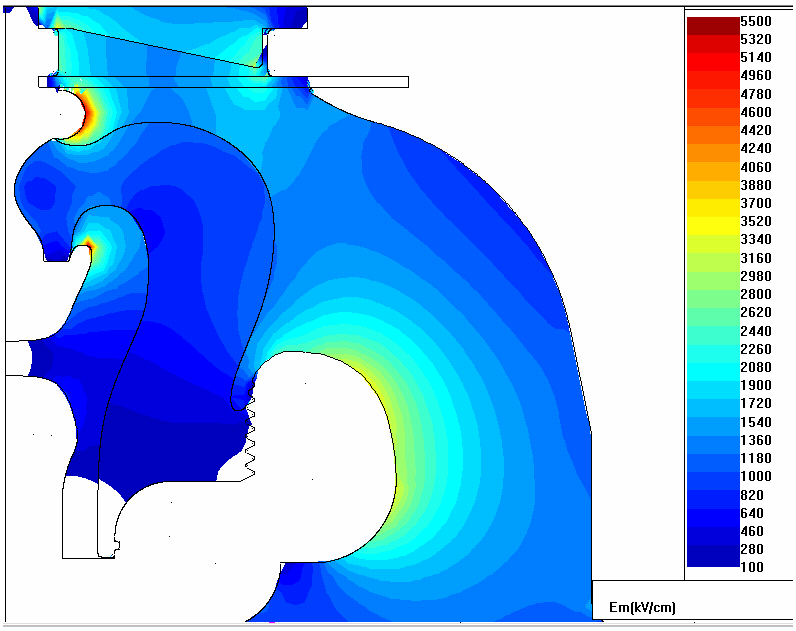

(b) Electric field distribution in JOLT transfer switch design in open mode

Figure 12. Critical electric field plots in JOLT transfer switch
(right of the transfer switch seen in figure 10 a)

The precise tolerances achieved on the high-pressure hydrogen switch clearly demonstrate the power of computer aided mechanical design in combination with material selection and accurate finite element analysis. All parts of the switch were fabricated directly from 3D CAD electronic data to hold the close tolerances required for a complete seal. Machining from electronic data allowed surfaces defined by mathematical equations to be created exactly to specification. All components were fully rendered and fit checked as a 3D solid model that eliminated assembly mismatches. In addition to a tight seal to the high pressure insulating media, manufacture from electronic data files allowed the electric field profiles to be calculated precisely as fabricated and a weakness in the prototyping process was eliminated.

The design of a 1 MV compact, high-pressure gas switch for high repetition rate operation has been detailed and demonstrated. A practical criteria for the inhibition of surface flashover along the high pressure gas/insulating solid interface has been successfully demonstrated under pulse repetition rates of 600 Hz. Excellent commercially available electrostatic field solvers enabled the use of complex interface shapes.

3.4 Peaking Section and Peaking Switch

Upon closure of the Hydrogen transfer switch, the transfer capacitor charges the peaking capacitor to 800 kV in approximately 2 ns. The oil peaking switch then closes and discharges the transfer and peaking capacitors into the 85 Ω antenna load. The peaking capacitor provides the fast risetime into the antenna and the transfer capacitor provides the 5 ns decay. Oil is chosen for use in the peaking switch for two primary reasons.

1) The breakdown field in oil is a strong function of the rise time of the applied voltage. The 2 ns charge time in the Jolt system allows the use of a peaking switch gap spacing of only 0.76 mm. The small gap spacing results in very low arc inductance and resistance. The resulting rise time of the wave front launched from the peaking switch is approximately 130 ps.

2) The Jolt peaking capacitor, peaking switch and antenna feed arms are all insulated with oil (ε_r = 2.25) and the oil is contained using polypropylene (ε_r = 2.3). The use of materials with equal dielectric constants throughout the fast rise time launching structure results in less waveform distortion than would be the case with multiple dielectric constants.

The final switch is a self-break, flowing-oil peaking switch, as shown in figure 13. The lower electrode of the peaking switch is charged to 800 kV in approximately 2 ns by the transfer switch and capacitor. The upper electrode is immediately transitioned to two antenna feed arm sections. The peaking capacitor is directly below the peaking switch, and is designed as a fast discharge coaxial capacitor. A 1 kΩ radial water resistor is incorporated to prevent charging of the peaking switch during the transfer capacitor charging phase. The flowing oil supply enters the peaking capacitor section immediately above the radial water resistor and flows through the ground plane insert, past the peaking switch and into the inner oil containment dome. The peaking switch requires 42 gallons/minute oil flow for proper operation at 200 Hz and 800 kV charge voltage.

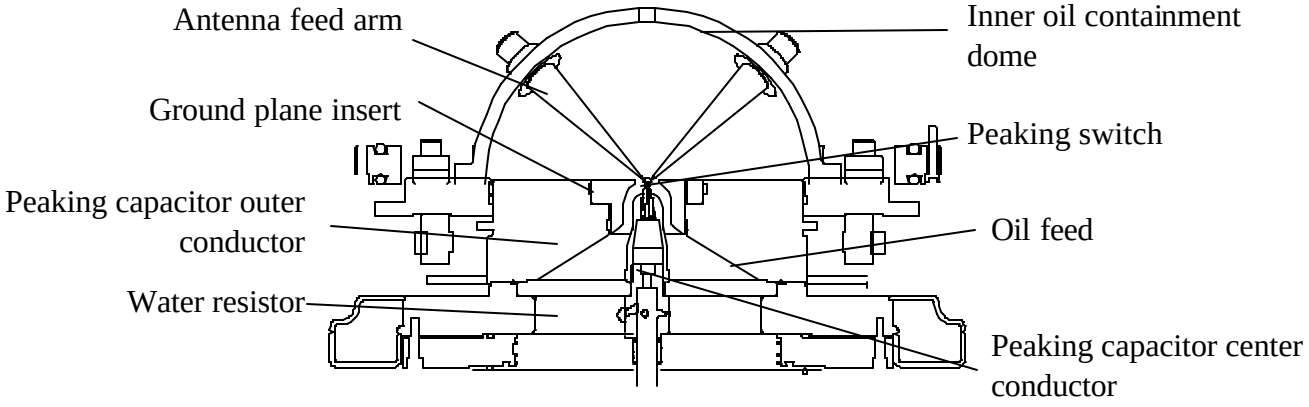

Figure 13. Geometrical details near the focal point of the reflector showing the feed-point lens

There were two major challenges in the implementation of the JOLT oil peaking switch.

1) There was significant difficulty in achieving the 42 gallons/minute oil flow through the switch and peaking capacitor to sustain the required 200 Hz PRR without inducing oil cavitations. Insufficient oil flow resulted in debris from switching events contaminating the oil in the peaking capacitor on subsequent switching events. This resulted in breakdown of the oil during the peaking capacitor charge phase after a number of switching events in a pulse train. The number of switching events into the pulse train at which the peaking capacitor insulating oil broke down was directly related to the peaking section oil flow rate. Breakdown of the peaking capacitor insulating oil results in shunting the pulse energy directly to ground.

2) The peaking switch structure is very small by design to limit pulse dispersion effects. This design necessitates the use of very small peaking switch electrodes; the upper switch electrode is essentially a 0.44 cm diameter sphere. The resulting electrode erosion rate necessitates adjusting the peaking switch after every 2,000 switching events to maintain the proper firing voltage.

Having completed the description of the pulser, we will now proceed to describe the half IRA in the following section.

4. Description and Analysis of the Half-IRA

4.1 Description of the Half-IRA

The JOLT antenna is a half-IRA with a 3.05m (10 feet) diameter, paraboloidal, commercial microwave reflector that has been cut in half and flanged for attachment to the ground plane. The transient energy source located at the focal point of this reflector launches a near-ideal TEM spherical wave on to the reflector through a polypropylene lens to be reflected as a collimated beam. A line schematic diagram and a photograph of the JOLT system are shown in figure 14. The ground plane creates rigidity for the upper surface of the modular frame and serves as the ground reference and an image plane for the impulse radiating antenna (IRA). It also provides the lower containment for SF6, which insulates the dome and feed arms. The ground plane also creates a shielded volume under it for the placement of sensitive components of the pulser. The gas containment bag is a clear, plastic dome constructed from flexible, UV-stabilized PVC film. This film is surrounded by a gas-tight zipper which fastens the bag to the edges of the ground plane and the perimeter of the antenna. The gas is filled from the back side of the antenna and the pressure is monitored by a sensitive, MagnaHelic pressure gauge. The Gas System supplies the high-pressure hydrogen gas to both the trigatron switch (300 psi) and the transfer switch (1,650 psi). The system is charged using high-pressure, sealable quick-disconnects which are connected to an external hydrogen gas cylinder. When the switches are charged to the correct pressure, a valve is closed to trap the gas in the system. The line pressure is then vented and the quick-disconnect released.

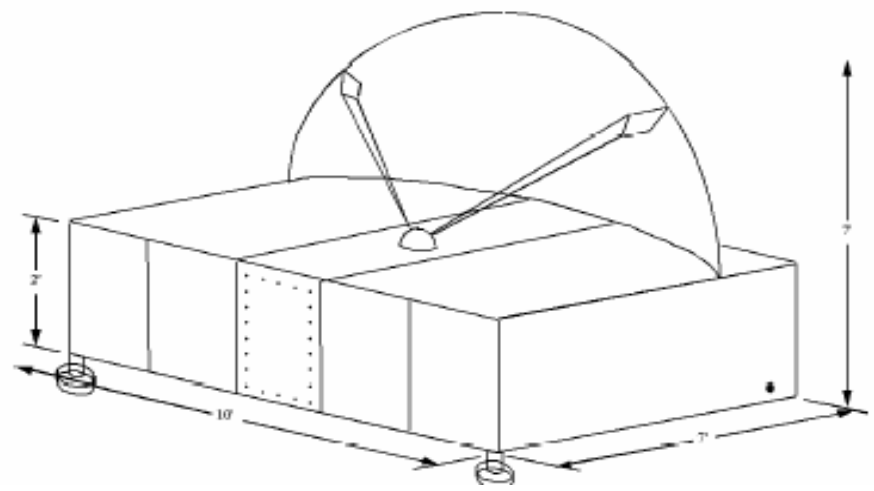

(a) Line schematic diagram

(b) Photograph of JOLT on a trailer

Figure 14. Line schematic (with dimensions) and a photograph of the JOLT hyperband system

Some of the ancillary systems that are part of the JOLT as a whole include:

Elevation System

The Elevation System works in conjunction with the rotational system to aim JOLT at the desired target. This system consists of a pulse DC motor driving a linear mechanical actuator. The entire system is mounted to the frame by two parallel shafts with linear bearings.

Environmental Control System

The Environmental Control System consists of the heating and air conditioning of the JOLT system for thermal management of the unit during operation. Controlling the temperature is very important because of the temperature limitations of the batteries, power supplies, transformer oil and other components. This is accomplished by the use of a high-quality yacht refrigeration system with digital controls for warm weather operation and auxiliary heating strips for cold weather operation.

Camera Mounting / EMI Window

JOLT positioning can be monitored by means of an internally mounted video camera that looks out through a metal-film EMI-shielded window. During testing, the camera's gimbaled mount can be adjusted so that the cross-hairs of the camera line up with the center of the radiated beam. The image is transmitted on channel 53 to a near-by television monitor. Precise positioning is accomplished via joy-stick over an RF control link.

Battery Support System

JOLT has the unique feature of relying on high-power battery packs as a power source rather than generators or external power cords. These battery packs are similar to those that were used in a record-breaking, high-speed electric car. This gives the unit increased mobility and self-containment, allowing its deployment without the encumbrance of additional equipment.

Getting back to the electromagnetic features of this unique radiator, we installed a polypropylene lens at the focal point to ensure a near-ideal spherical TEM wave launch on to the conical transmission lines formed by the feed arms.

The spherically shaped (for mechanical ease of construction) feed-point lens with a radius of 0.457 m (18") serves three purposes.

(a) It ensures a near-ideal spherical TEM launch on to the reflector
(b) Because of its polypropylene construction, it provides the necessary insulation between the feed arms and the ground plane.
(c) It provides an inner containment dome for the high-velocity transformer oil, which is used to clear debris from the peaker switch.

The electric fields inside the lens are held-off by the oil insulating medium. However, outside the spherical lens medium, we have SF_6 gas at 1 atmosphere pressure and the electric field has "hot spots" or field maxima around the feed arm conductor protruding out of the lens. These local field enhancements were estimated using the expressions in [17] and the lens diameter (36") and the initial impedance (85W) were chosen so that any electrical breakdowns around these field enhancement points were prevented. The interface between the lens and the outside gas medium could have two dielectric discontinuities (oil/container and container/gas). We eliminated one of these discontinuities by choosing polypropylene container material that has the same dielectric constant as the oil. It is possible to shape the container geometry [5] so as to obtain the desired spherical wavefront centered at the focal point. We initially computed this ideal container or the lens profile, but it turned out to be mechanically large and unwieldy. For ease of fabrication and to keep the lens size practical, an engineering compromise was made to use a spherical lens. It is noted that the spherical shape of the electromagnetic lens is not the ideal shape, since the dielectric discontinuity (2.25 to 1) reflects the energy back to the focal point at the same instant of time. The more ideal, on-spherical shaped lens employed in [5] tends to diffuse these reflections. The lens does have another useful effect. The dielectric discontinuity causes an impedance mismatch at the lens exit surface. The net characteristic impedance jumps from 85 W in the oil medium to 100 W in outside SF_6 gas medium, resulting in a voltage bump up by about 8 %.

The feed arms radiate from a small diameter metal sphere which forms the upper electrode of the peaker switch. When this switch breaks down, the electrical pulse is carried by the two feed arms and is terminated at the IRA with a resistance box. The resistance box contains HVR ceramic resistors [18]. The prescribed conical angle of the feed arms minimizes diffractions of the wave scattered by the reflector by providing a uniform outer surface to carry the pulse.

4.2 Boresight Field Analysis of the Half IRA

Mikheev et al., [19] have proposed a simple method for calculating the near, intermediate and far fields of the reflector IRA, within some constraints. Basically, this method uses the conical transmission-line fields reflected in the parabolic mirror. If the antenna was a flat plate, the conical transmission-line would have an identical mirror image in the flat plate, resulting in the feed line and its image having the same expansion angle. However, since the antenna is paraboloidal in shape, the image is also a conical transmission line with a different expansion angle. The various geometrical parameters for boresight field calculations are shown in figure 15.

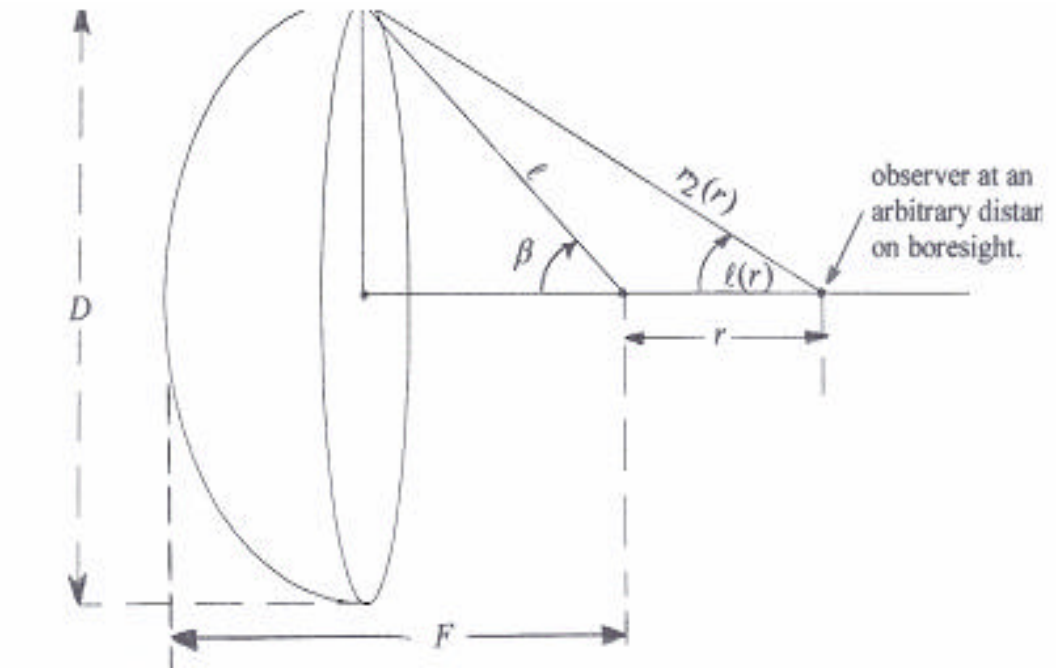

Figure 15. The geometry for the boresight field calculations

The total electric field at any point on the boresight axis, at a distance of *r* from the focal point is given by

$$E(r,t) = -\frac{1}{2 f_g p}\left[\begin{array}{l} \dfrac{V\left(t-\dfrac{r}{c}\right)}{r}\,\dfrac{\sin(b)}{1+\cos(b)} \\ -\dfrac{V\left(t-\dfrac{\ell}{c}-\dfrac{r_2}{c}\right)}{r_2}\,\dfrac{\sin(b)+\sin(g)}{1+\cos(b-g)} \\ -\dfrac{4V\left(t-\dfrac{2F}{c}-\dfrac{r}{c}\right)}{D} \\ -(2+2\cos(g))\dfrac{V\left(t-\dfrac{\ell}{c}-\dfrac{r_2}{c}\right)}{D} \end{array}\right] \tag{1}$$

where the geometric impedance factor f_g is the ratio of the antenna input impedance Z_c to the characteristic impedance of free space Z_0, or $f_g = (Z_c / Z_0)$. It is noted that for a paraboloidal reflector,

$$\frac{\sin(b)}{1+\cos(b)} = \frac{D}{4F} \tag{2}$$

The above expression contains the voltage V(t) launched on to the antenna plates. This expression can be specialized to give boresight far fields and can also be specialized for half IRAs. We have further verified that when the range parameter r is in the far field the expression in (1) reduces to the familiar expression in [20]

$$E(r,t) \cong \frac{D}{4p\, r c\, f_g}\left[\frac{\partial V\left(t-\dfrac{2F}{c}-\dfrac{r}{c}\right)}{\partial t} - \frac{c}{2F}\left\{V\left(t-\frac{r}{c}\right)-V\left(t-\frac{2F}{c}-\frac{r}{c}\right)\right\}\right] \tag{3}$$

The far field expression of (3) is valid for a full IRA with a single conical feed line, when the range r satisfies the far field criterion,

$$\text{range} \quad r \geq \left(\frac{D^2}{2 c\, t_{mr}}\right) \tag{4}$$

where D is the diameter of the reflector, c = speed of light in vacuum and t_{mr} is the maximum rate of rise of the voltage wave launched on to the reflector. The far field criterion of (4) is derivable from requiring that the antenna clear time be at least one-fourth of the risetime. For example, for the prototype IRA [5], D = 3.66 m and the risetime was ~ 100 ps, resulting in the far field starting from a distance of about 225 m. Examining the two parts of (3), it is well established that the second term is the prepulse or the direct radiation from the source at the focal point and the first term is the impulse part radiated by the reflector into the far field. Of course, the prepulse and the impulse are of opposite signs and have a net zero area to ensure no DC radiation into the far field. Looking at the impulse portion and specializing it to the present case of a half IRA fed by a pair of conical lines, we arrive at the following expression for the ($r E_{far}$)

$$r E_{far}(r,t) = \left(\frac{D}{4\sqrt{2}}\right)\frac{1}{2p\ c\ f_g}\ \frac{dV(t)}{dt} \tag{5}$$

Substituting the JOLT parameters of D = 3.048 m, f_g ~ (100/ 377) = 0.265 and the constant c = 3 x 10^8 m/s, we have

$$\left(r E_{far}\right)(peak) = 1.082\ x\ 10^{-9}\left(\frac{dV}{dt}\right)_{\max}\ \text{Volts} \tag{6}$$

The maximum rate of rise in the above expression refers to the voltage wave launched on to the reflector. This is a relatively difficult number to obtain from the measurements. Typically the pulser diagnostic waveforms are in some section of the pulser, e.g., peaking section voltage waveform and by the time the voltage is launched on to the reflector, it does undergo some changes both in amplitude and in risetime. One can take either of the following two approaches to get the maximum rate of rise of the voltage waveform.

a) measure the waveform with a ground plane sensor at or near the center of the reflector and deduce the maximum rate of rise from it, or
b) measure the left hand side of (6) by measuring the radiated electric field on boresight at some far field distance and then derive the maximum rate of rise of the voltage waveform launched.

Before we present the measured results, we can use (6) and estimate the peak value of ($r\ E_{far}$) for a range of maximum rate of rise, as listed in Table 3.

TABLE 3. Achievable peak values of ($r\ E_{far}$) for assumed maximum rate of rise

Case #	Assumptions about the maximum rate of rise of the voltage waveform launched on to the reflector	Peak value of ($r\ E_{far}$) from equation (6) = $1.08 \times 10^{-9}\ (dV/dt)_{max}$	"Gain" ($r\ E_{far}$) / V_p
1	V_p = 800 kV ; t_{mr} = 200 ps (dV/dt) max ~ 4×10^{15} V/s	**4.32 MV**	**5.4**
2	V_p = 800 kV ; t_{mr} = 160 ps (dV/dt) max ~ 5×10^{15} V/s	**5.40 MV**	**6.75**
3	V_p = 1 MV ; t_{mr} = 200 ps (dV/dt) max ~ 5×10^{15} V/s	**5.40 MV**	**5.4**
4	V_p = 1 MV ; t_{mr} = 180 ps (dV/dt) max ~ 5.556×10^{15} V/s	**6.0 MV**	**6.0**
5	V_p = 1 MV ; t_{mr} = 150 ps (dV/dt) max ~ 6.667×10^{15} V/s	**7.2 MV**	**7.2**

One immediately observes that ($r\ E_{far}$ / V_p) is certainly greater than 1 and it happened to be a little over 10 for the prototype IRA [5]. It is worth noting that there are factors such as the voltage bump-up from the lens (8 %) which increases the voltage out of the peaking section launched on to the reflector. On the other hand, there are factors such as the fill factor of the reflector (how uniformly the spherical TEM wave illuminates the reflector), and the blockage of the aperture due to the lens and other objects in front of it tend to decrease the time domain peak in the far field, by several percent. Simple expressions such as (6) can not account for these factors. Not withstanding these factors, the **($r\ E_{far}$)** for case # 4 indicated in Table 3 above are in the right range of observation in JOLT.

4.3 **A Realistic Model for the JOLT Pulser Waveform**

Transient pulse generators are typically specified with three numbers. They are: peak amplitude, the (10-90)% risetime and the FWHM. Such a characterization is inadequate in the context of an impulse radiating antenna, where the far field is proportional to the maximum rate of rise of the voltage waveform launched on the antenna. This voltage could be different from the voltage out of the pulser owing to the presence of other dielectric media at the feed point. It then becomes important to assess the maximum value of the voltage rate of rise. So, instead of the usual double exponential model, we have used the following analytical model [6]. The pulser voltage, its derivative and the Fourier transform are given by:

$$\begin{aligned} V(t) &= V_0\, e^{-\frac{b\,t}{t_d}}\left[\left(\frac{1}{2}\right) erfc\left(\sqrt{p}\,|t|/t_d\right)\right] \quad t<0 \\ &\quad V_0\, e^{-\frac{b\,t}{t_d}}\left[1-\left(\frac{1}{2}\right) erfc\left(\sqrt{p}\;t/t_d\right)\right] t>0 \end{aligned} \tag{7}$$

$$\frac{dV(t)}{dt} = \frac{V_0}{t_d}\, e^{-b\left(\frac{t}{t_t}\right)}\; e^{-p\left(\frac{t}{t_d}\right)^2} - \frac{b}{t_d} V(t) \tag{8}$$

$$\tilde{V}(w) = \frac{V_0\, t_d}{(b + jwt_d)}\; e^{\left[\frac{1}{4p}(b\,+\,jwt_d)^2\right]} \tag{9}$$

The above analytical model of the pulser, although still characterized by three numbers, has continuous derivatives and typical pulser outputs are well represented by this model. These numbers for the JOLT pulser are:

V_0 = 1.025 MV, t_d = 180 ps, beta = 0.036 = (rise / exponential decay) = (180 ps / 5 ns) (10)

The resulting maximum rate of rise for this pulser is (dV/dt) max = 5.556 x 10^{15} V/s.

The above outlined pulser model is used in computing the boresight fields at various distances, by substituting this voltage waveform into (1) from [19]. The results are shown in figures 16 to 20. Figure 16 shows the analytical model for the voltage waveform launched on to the antenna, where one can see the peak amplitude of 1 MV and an exponential decay of 5 ns. The voltage waveform is re-plotted in figure 17 on a log-linear scale to exhibit the smooth rise or a continuous derivative and a maximum rate of rise of 180 ps. The magnitude of the frequency spectrum of the applied pulse model is shown in figure 18. Being a mono-polar pulse, it does have a lot of DC content, as can be seen in this figure. As a function of frequency, the applied pulse is a constant at low frequencies, falls of like (1/f) at mid range and then falls off more rapidly ($1/ f^2$) at high frequencies. Since the far field is the time derivative of the applied voltage, the far field spectral magnitude will be proportional to $| w \tilde{V}(w) |$ resulting in an extremely wide band of radiated spectral fields. The far field is estimated to start at a range *r* given by (4) to be r $\geq$ 85 m.

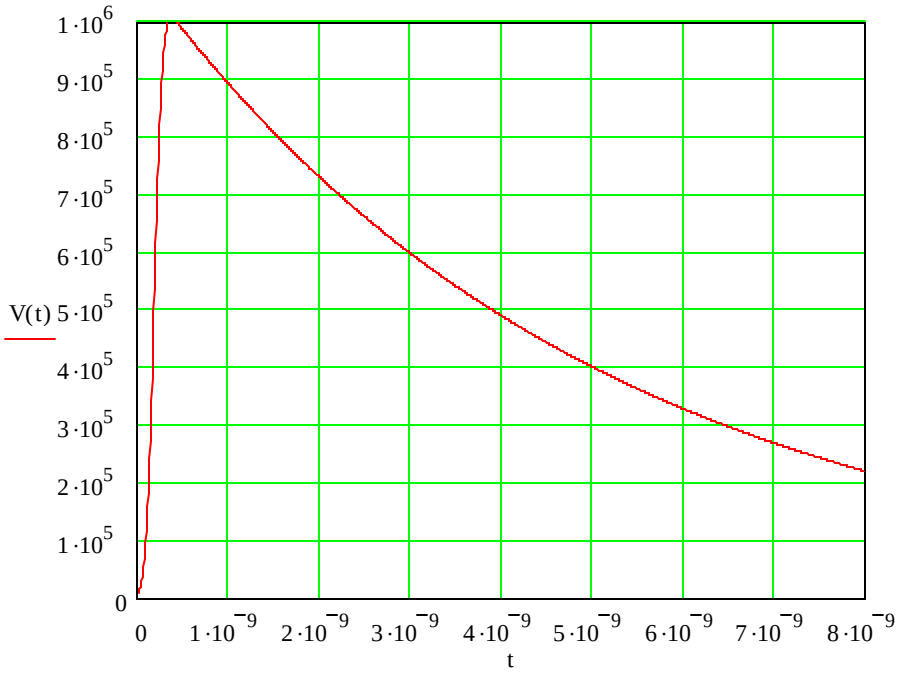

Figure 16. The "ideal" voltage waveform used in analysis

Pulser Output (Peak= 1 MV, rise 180ps, Exponential Decay = 5 ns)

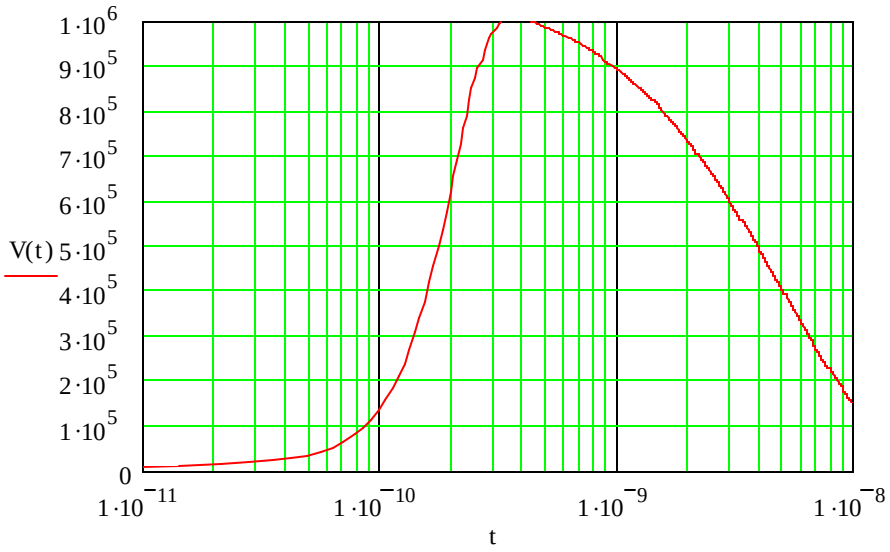

Figure 17. Rise and decay with maximum rate of rise 180 ps exhibiting continuous derivative

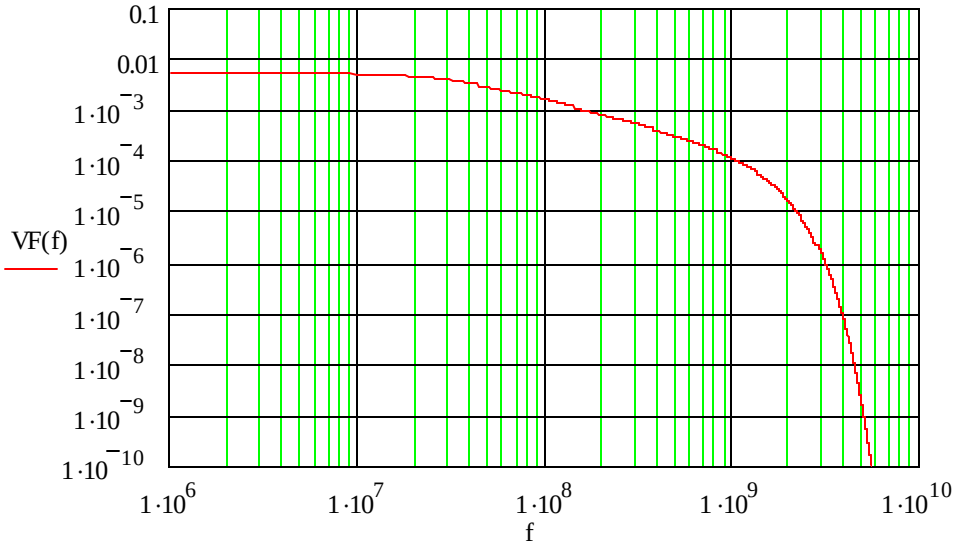

Figure 18. Magnitude Spectrum of the applied pulse

Using the analytical model of the voltage waveform shown in figures 16-18, which is at best an estimate of the expected waveform out of the JOLT pulser, we can now proceed to estimate the near, intermediate and far fields on the boresight axis. This is done using the analytical voltage waveform in (1). The results are shown in figures 19 and 20. Figure 19 has the time domain electric fields at various distances and figure 20 has the corresponding spectral magnitudes.

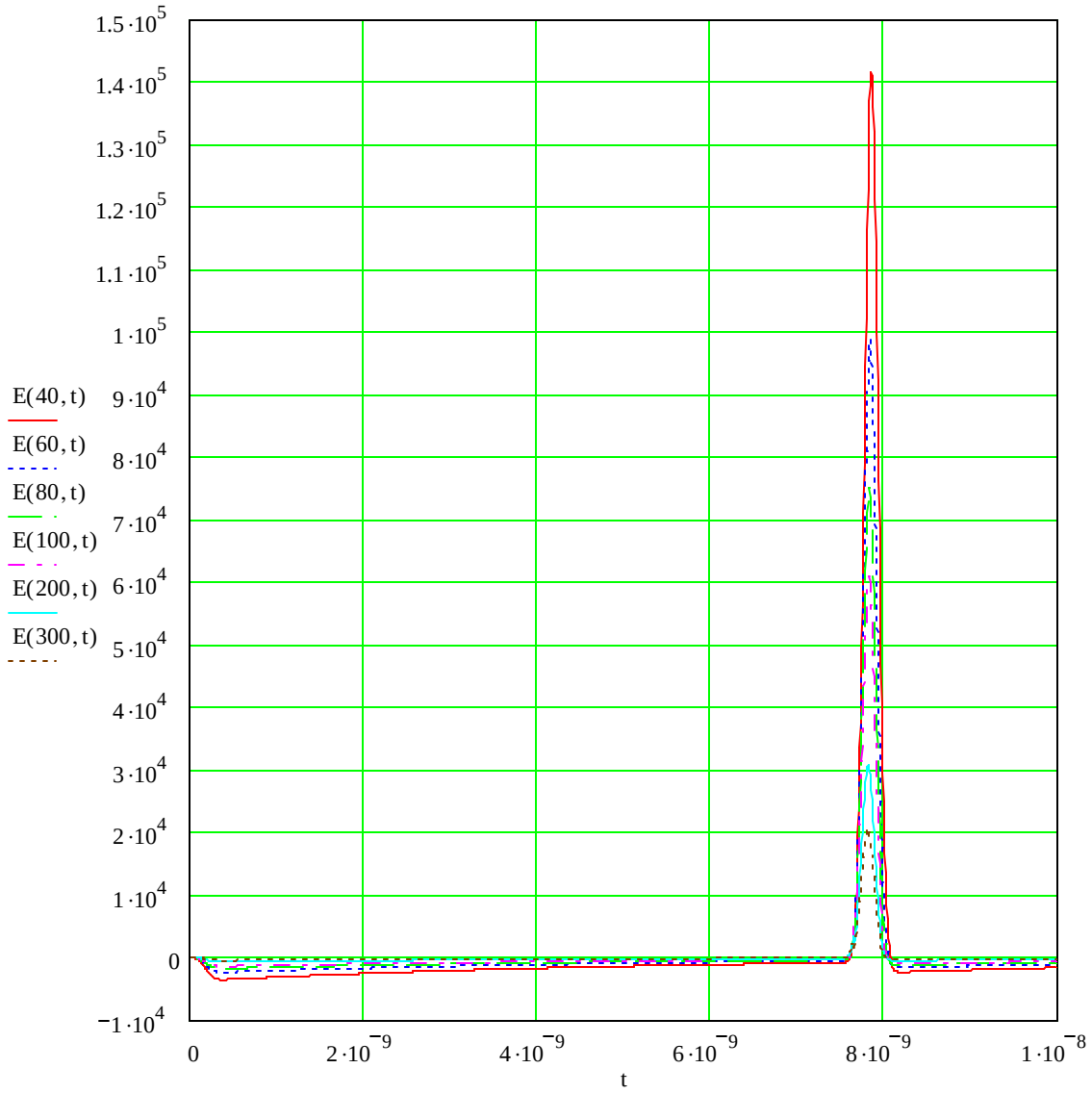

Figure 19. Boresight electric fields at various distances

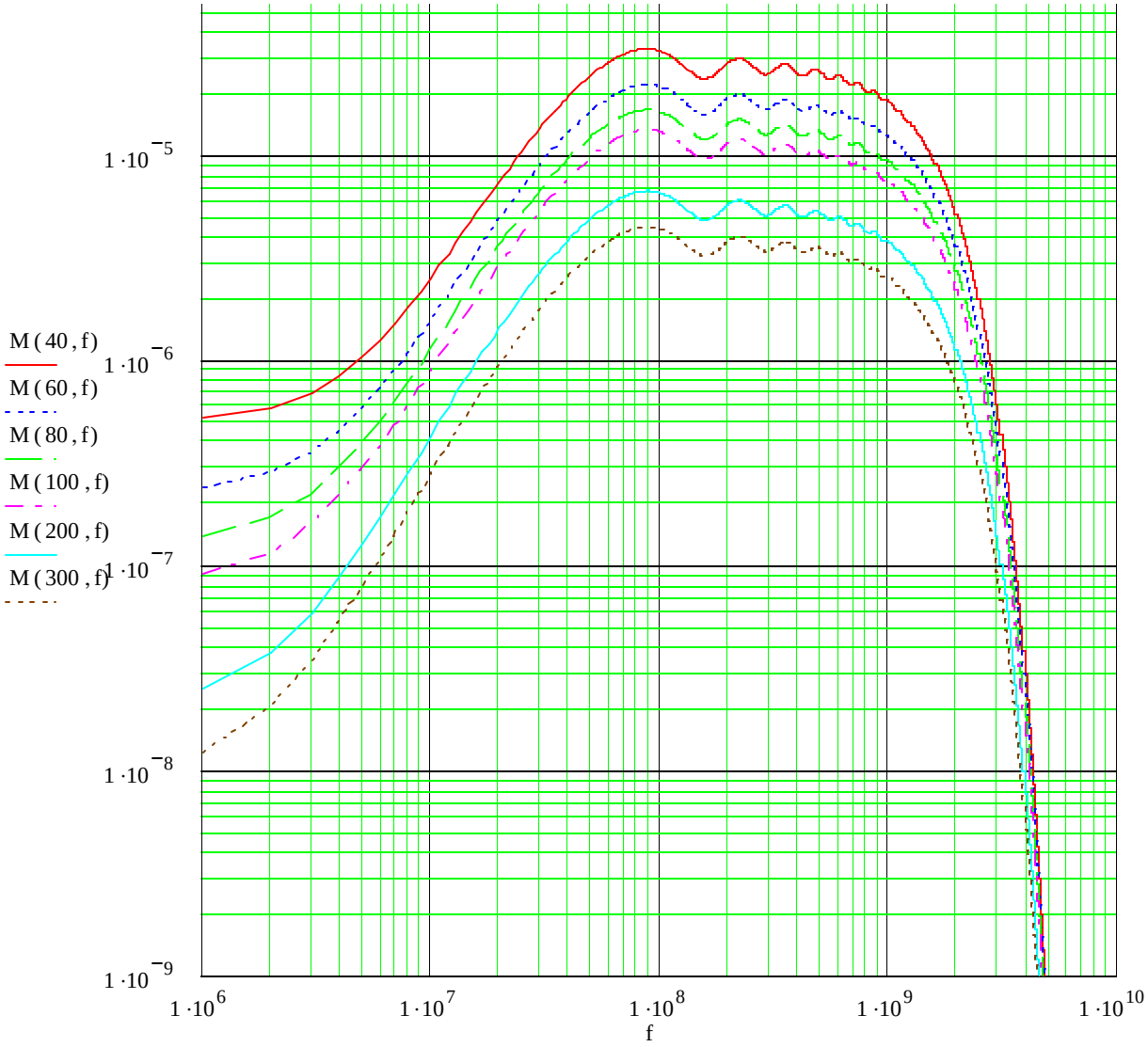

Figure 20 . Magnitude Spectrum of the boresight electric field at various distances

From the results of figure 19, it is observed that at a range of 100m for example, which is certainly in the far field, the peak electric field is ~ 60 kV/m and consequently the **(*r E far*)** is about 6 MV. It is seen that this value of **(*r E far*)** is in agreement with the simple calculation shown as case# 4 of Table 3, which just confirms that (1) reduces to (3), on boresight in the far field. The actual measured value was a peak boresight electric field of 62 kV/m at a distance of 85m, resulting in a **(*r E far*)** from measurement of 5.3 MV, pointing out that the peak (dV/dt) is ~ 5 x 10^{15} V/s.

5. Experimental Data

One sample measured data from JOLT can be seen in figure 21. It is a measurement of the electric field on boresight at a distance of 85m, with a peak electric field of ~ 62 kV/m yielding a $(r\ E_{far})$ of 5.3 MV. If one considers the value of electric field going from the negative to positive peak, it is ~ 80 kV/m at 85 m resulting in $(r\ E_{far})$ of ~ 6.8 MV. This is a matter of interpretation.

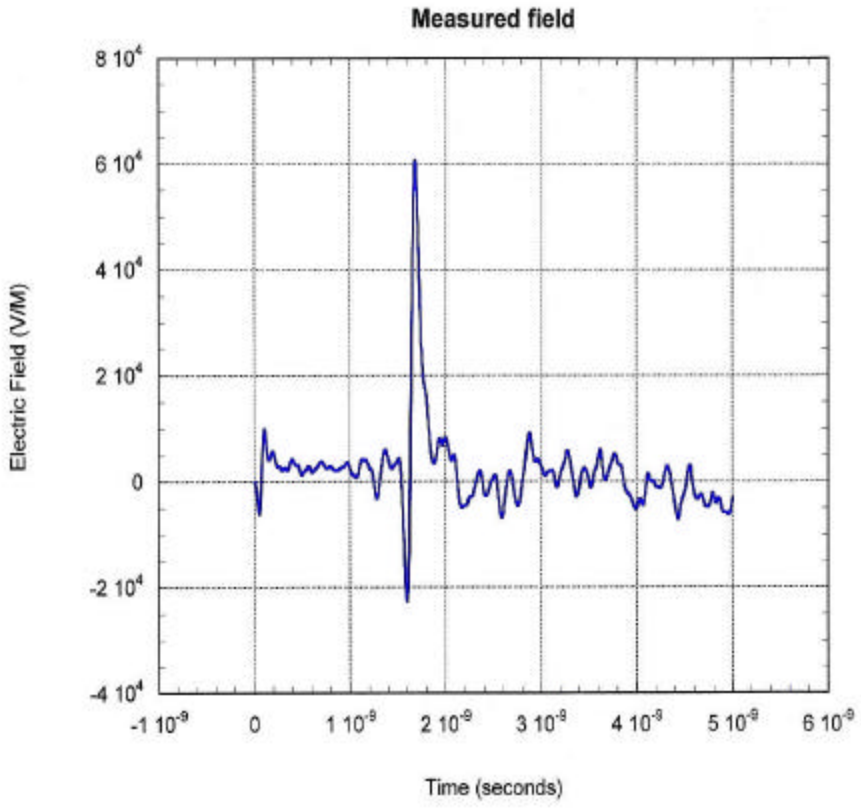

Figure 21. Measured electric field at a boresight distance of r = 85m

One can compare the measured waveform in figure 21 to the calculated value in figure 19. In doing this comparison, several comments about the calculations and the measurement are in order.

a) The calculated electric field waveform is an ideal situation considering an analytical pulser model.

b) The calculations display a prepulse as expected lasting a duration of about (2 F / c) with F being the focal length and c being the speed of light in vacuum.

c) The calculations do not account for factors such as aperture blockage, diffraction from plate edges and the semi-circular rim of the reflector. In some sense, the assumed value of (dV/dt) maximum takes care of these effects. In other words, we do not exactly know the (dV/dt) maximum in the voltage waveform; one can derive this as a parameter to match the observed time domain peak in the far field. When we matched the time domain peak, the (dV/dt) came out to be ~ 5 x 10^{15} V/s, which is a reasonable number for JOLT, from its design parameters.

d) The calculated waveform correctly shows that the prepulse and impulse are of opposite signs.

e) The calculated waveform also displays equal areas under the prepulse and the impulse, as expected.

f) The measured waveform does not cleanly capture the prepulse.

g) The measured waveform has a negative spike, just prior to the positive impulse, which is caused by some imperfection in the rise portion of the voltage waveform.

h) Since the far electric field is the time derivative of the applied voltage, the time integral of the measured electric field is an indication of the voltage pulse shape. Ideally, if one considers the prepulse in its entirety and the impulse, the field should integrate out to zero (no DC in the radiated field).

i) A possible explanation for the negative spike in the impulse portion is a potential stray capacitance in the peaking switch, which could be addressed in future measurements of the JOLT system.

6. Summary

In this note, we have described a large, high voltage transient system built at the Air Force Research Laboratory, Kirtland AFB, NM. The pulsed power system centers around a very compact resonant transformer capable of generating over 1 MV at a pulse repetition rate PRF of 600 Hz. This is switched, via an integrated transfer capacitor and an oil peaking switch onto an 85-W Half-IRA (Impulse Radiating Antenna). This unique system will deliver a far radiated field with a risetime of near 80 ps, a FWHM on the order of 100 ps, and a field-range product (r E_{far}) of ~ 5.3 MV, exceeding all previously reported results by a factor of several. The radiate field has a fairly flat spectrum from about 50 MHz to about 2 GHz (see figure 20). The lower frequency limit is governed by the reflector size, when the diameter of the reflector becomes ~ (1/2) wavelength, it is no longer an efficient radiator. The upper frequency limit is governed by the risetime of the voltage pulse launched on to the reflector. JOLT is indeed an intensive, hyperband radiator that is expected to find many applications.

References

1. W. D. Prather, C. E. Baum, F. J. Agee, J. P. O'Laughlin, D. W. Scholfield, J. W. Burger, J. Hull, J. S. H. Schoenberg and R. Copeland, "Ultrawide Band Sources and Antennas: Present Technology, Future Challenges" *Ultra-Wideband, Short Pulse Electromagnetics 3*, C. E. Baum, L. Carin and A. P. Stone Editors, pp 43-56, Plenum Press, NY, 1997.

2. Short Form Catalog, Picosecond Pulse Labs, Inc., Boulder, CO, www.picosecond.com

3. Short Form Pulsers, Kentech Instruments Ltd., Didcot, Oxfordshire, U.K., www.kentech.co.uk

4. Operations Manual for HYPS Pulse Source, Grant Applied Physics, Inc., San Francisco, CA.

5. D. V. Giri, H. Lackner, I. D. Smith, D. W. Morton, C. E. Baum, J. R. Marek, W. D. Prather and D. W. Scholfield, "Design, Fabrication and Testing of a Paraboloidal Reflector Antenna and Pulser System for Impulse-Like Waveforms", IEEE Trans. Plasma Sciences, volume 25, pp 318-326, April 1997.

6. D. V. Giri, J. M. Lehr, W. D. Prather, C. E. Baum and R. J. Torres, "Intermediate and Far Fields of a Reflector Antenna Energized by a Hydrogen Spark-Gap Switched Pulser, IEEE Trans. Plasma Sciences, volume 28, pp 1631-1636, October 2000.

7. C. E. Baum, E. G. Farr and D. V. Giri, "Review of Impulse-Radiating Antennas," chapter 16, pp 403-439, in W. R. Stone (editor), *Review of Radio Science 1996-1999*, Oxford University Press.

8. C. J. Buchenauer, J. S. Tyo and J. S. H. Schoenberg, "Antennas and Electric Field Sensors for Ultra-Wideband Transient Time Domain Measurements: Applications and Methods" *Ultra- Wideband, Short Pulse Electromagnetics 3*, pp 405-422, Plenum Press, New York, 1997.

9. C. E. Baum, "Configurations of TEM Feed for an IRA," Sensor and Simulation Note 327, 27 April 1991.

10. C. E. Baum, "Variations on the Impulse Radiating Antenna Theme," Sensor and Simulation Note 378, February 1995.

11. E. G. Farr and C. E. Baum, "Feed-Point Lenses for Half-Reflector IRAs," Sensor and Simulation Note 385, November 1995.

12. J. S. Tyo and J. S. H. Schoenberg, "Radiated Field Measurement from a 1-m Diameter Half IRA," Sensor and Simulation Note 471, February 1999.

13. F. Sabath, D. Nitsch, M. Jung, Th. H. G. G. Weise, "Design and Setup of a short Pulse Simulator for Susceptibility Investigations," Sensor and Simulation Note 460, 1 October 2001.

14. D. V. Giri, "Classification of Intentional EMI (IEMI) Based on Bandwidth," Presented at AMEREM 2002, Annapolis, MD, 2-7 June 2002.

15. J. M. Lehr, M. D. Abdalla, F. Gruner, M. C. Skipper and W. D. Prather, "Development of a Hermetically sealed, High-Energy Trigatron Switch for High Repetition Rate Applications," 12th IEEE International Pulse Power Conference, 1999, Monterey, CA, June 27-30, 1999, pp 146-149.

16. J. M. Lehr, M. D. Abdalla, J. W. Burger, J. M. Elizondo, J. Fockler, F. Gruner, M. C. Skipper, I. D. Smith and W. D. Prather, "Design and Development of a 1 MV, Self Break Switch for high Repetition Rate Operation," 12th IEEE International Pulse Power Conference, 1999, Monterey, CA, June 27-30, 1999, pp 1199-1202.

17. E. G. Farr and G. D. Sower, "Design Principles of Half-Impulse Radiating Antennas, Sensor and Simulation Note 390, December 1995.

18. J. M. Lehr, J. W. Burger, W. D. Prather, J. Hull, M. D. Abdalla, M. C. Skipper and D. V. Giri, " Evaluation of Resistors for Transient High-Voltage Applications," 12th IEEE International Pulse Power Conference, 1999, Monterey, CA, June 27-30, 1999, pp 666-669.

19. O. V. Mikheev et al., "New Method for Calculating Pulse Radiation from an Antenna with a Reflector", IEEE Transactions on Electromagnetic Compatibility, volume 39, number 1, February 1997, pp 48-54.

20. C. E. Baum, "Radiation of Impulse-Like Transient Fields", Sensor and Simulation Note 321, 25 November 1989.